Crystals **2012**, *2*, 1502-1513; doi:10.3390/cryst2041502

OPEN ACCESS

crystals

ISSN 2073-4352

www.mdpi.com/journal/crystals

Article

Magnetism and Pressure-Induced Superconductivity of Checkerboard-Type Charge-Ordered Molecular Conductor *β*-(*meso*-DMBEDT-TTF)$_2$X (X = PF_6 and AsF_6)

Takahisa Shikama [1], Tatsuya Shimokawa [1], Sanguchul Lee [1], Takayuki Isono [1], Akira Ueda [1], Kazuyuki Takahashi [2], Akiko Nakao [3], Reiji Kumai [4], Hironori Nakao [4], Kensuke Kobayashi [4], Youichi Murakami [4], Motoi Kimata [1], Hiroyuki Tajima [1], Kazuyuki Matsubayashi [1], Yoshiya Uwatoko [1], Yutaka Nishio [5], Koji Kajita [5] and Hatsumi Mori [1,*]

1 The Institute for Solid State Physics, The University of Tokyo, Kashiwa, Chiba 277–8581, Japan; E-Mails: tshikama@issp.u-tokyo.ac.jp (Tak.S.); tshimokawa@issp.u-tokyo.ac.jp (Tat.S.); sangchul@issp.u-tokyo.ac.jp (S.L.); tisno@issp.u-tokyo.ac.jp (T.I.); a-ueda@issp.u-tokyo.ac.jp (A.U.); kimata@issp.u-tokyo.ac.jp (M.K.); tajima@issp.u-tokyo.ac.jp (H.T.); kazuyuki@issp.u-tokyo.ac.jp (K.M.); uwatoko@issp.u-tokyo.ac.jp (Y.U.)

2 Department of Chemistry, Graduate School of Science, Kobe University, Kobe, Hyogo 657–8501, Japan; E-Mail: ktaka@crystal.kobe-u.ac.jp

3 Research Center for Neutron Science and Technology, CROSS, Tokai–mura 319–1106, Japan; E-Mail: a_nakao@cross.or.jp

4 Condensed Matter Research Center and Photon Factory, Institute of Materials Structure Science, KEK, Tsukuba 305–0801, Japan; E-Mails: reiji.kumai@kek.jp (R.K.); hironori.nakao@kek.jp (H.N.); kensuke.kobayashi@kek.jp (K.K.); youichi.murakami@kek.jp (Y.M.)

5 Department of Physics, Toho University, Chiba 274-8510, Japan; E-Mails: nishio@ph.sci.toho-u.ac.jp (Y.N.); kajita@ph.sci.toho-u.ac.jp (K.K.)

***** Author to whom correspondence should be addressed; E-Mail: hmori@issp.u-tokyo.ac.jp; Tel./Fax.: +81-4-7136-3444.

Received: 12 September 2012; in revised form: 5 November 2012 / Accepted: 14 November 2012 / Published: 29 November 2012

Abstract: The metallic state of the molecular conductor *β*-(*meso*-DMBEDT-TTF)$_2$X (DMBEDT-TTF = 2-(5,6-dihydro-1,3-dithiolo[4,5-*b*][1,4]dithiin-2-ylidene)-5,6-dihydro-5,6-dimethyl-1,3-dithiolo[4,5-b][1,4]dithiin, X = PF_6, AsF_6) is transformed into the checkerboard-type charge-ordered state at around 75–80 K with accompanying metal-insulator (MI) transition on the anisotropic triangular lattice. With lowering temperatures, the magnetic susceptibility decreases gradually and reveals a sudden drop at the MI

transition. By applying pressure, the charge-ordered state is suppressed and superconductivity appears in *β*-(*meso*-DMBEDT-TTF)$_2$AsF$_6$ as well as in the reported *β*-(*meso*-DMBEDT-TTF)$_2$PF$_6$. The charge-ordered spin-gapped state and the pressure-induced superconducting state are discussed through the paired-electron crystal (PEC) model, where the spin-bonded electron pairs stay and become mobile in the crystal, namely the valence-bond solid (VBS) and the resonant valence bonded (RVB) state in the quarter-filled band structure.

Keywords: superconductor; dimer state; checkerboard-type charge ordering; singlet state; valence bond solid; paired-electron crystal

1. Introduction

Recently, molecular conductors have attracted much interest as highly correlated electron systems. Most molecular charge transfer (CT) complexes have $[(\text{donor})_2]^{1+}$: $(\text{anion})^{1-}$ = 2:1 stoichiometry and a 3/4-filled band structure. The strongly dimerized system shows the dimer Mott state with an effective 1/2-filled band for *κ* and *β*′-type BEDT-TTF complexes, whereas the non-dimerized one reveals the charge-ordered state for *θ*-type complexes [1,2]. In order to obtain a variety of electronic states, the correlation parameters have been changed systematically by modifying the BEDT-TTF molecule. As a result, BEDT-TTF derivatives and their charge transfer complexes have been synthesized and prepared, and their physical properties have been investigated [3–9].

Among the CT salts based on BEDT-TTF derivatives, the complex *β*-(*meso*-DMBEDT-TTF)$_2$PF$_6$ with 3/4-filled band structure shows relatively weak metallic behavior from room temperature to 75 K and at an ambient pressure (Figure 1, [4,7]). The distinct metal-insulator transition occurs at 75 K, where the checkerboard-type charge ordering (CO) appears by accompanying the lattice distortion [5,6]. The charge disproportionation was also confirmed to be $D^{0.25+}D^{0.75+}$ from $D^{0.5+}D^{0.5+}$ [D = *meso*-DMBEDT-TTF] by IR and Raman spectroscopy [9]. By applying weak pressure, the superconducting (SC) transition occurs at T_c = 4.6 K under 0.06 GPa. The origin of the checkerboard-type charge-ordering pattern can not be explained only by Coulomb interaction [6]. The relation between the CO and the superconductivity is also under question. In order to clarify the origin of the checkerboard-type CO and its relation to the superconductivity, the preparation, the crystal structure analysis at 30 K, and the electrical and the magnetic properties of *β*-(*meso*-DMBEDT-TTF)$_2$AsF$_6$ were investigated in addition to the PF$_6$ complex [3–9].

Figure 1. (**a**) Molecular structure of *meso*-DMBEDT-TTF and (**b**) temperature dependence of the electrical resistivity under pressure for *β*-(*meso*-DMBEDT-TTF)$_2$PF$_6$ [4,6,7].

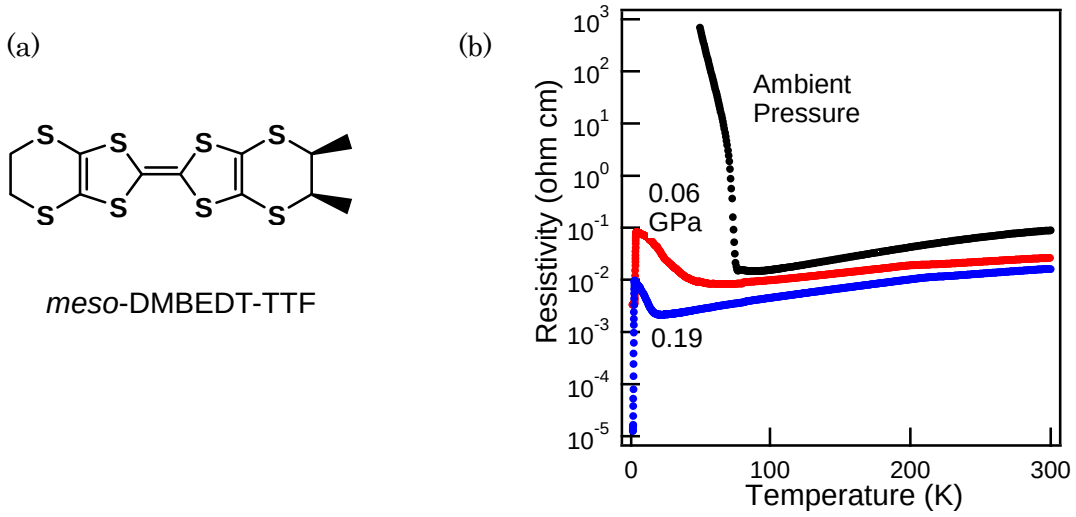

2. Results and Discussion

2.1. Metallic State at 298 K to Charge-Ordered State at 30 K for β-*(meso-DMBEDT-TTF)$_2$AsF$_6$*

The complex *β*-(*meso*-DMBEDT-TTF)$_2$AsF$_6$ is isostructural to the complex *β*-(*meso*-DMBEDT-TTF)$_2$PF$_6$ both at 298 K and 30 K. At 298 K, the crystallographically independent molecules are one donor and a half anion. Below 70 K, the unit cell is doubled, so that there are two crystallographically independent donors and one anion; the equivalent donors ($D^{0.5+}$ $D^{0.5+}$) in a dimer at 298 K are transformed to the charge-disproportionated donors ($D^{0.65+}$ $D^{0.35+}$), which are in the charge—rich $D^{0.65+}$ and the charge—poor $D^{0.35+}$ states (Figure 2, Table 1). Between dimers, two charge—rich $D^{0.65+}D^{0.65+}$ and two charge—poor $D^{0.35+}D^{0.35+}$ are adjacent, such as in $\cdot\cdot D^{0.65+})(D^{0.65+}D^{0.35+})(D^{0.35+}\cdot\cdot$ in the stacking direction, and construct the checkerboard-type charge-ordered state. Although the charge-ordered patterns of the PF_6 and the AsF_6 complexes are similar, the degree of charge disproportionation is relaxed from $D^{0.75+}D^{0.25+}$ for the PF_6 complex to $D^{0.65+}D^{0.35+}$ for the AsF_6 complex. As an anion size increases from PF_6^- to AsF_6^-, the unit cell volume at 298 K gets larger from 906(2) Å^3 [4] to 914.3(7) Å^3 and the dimerization ratio *r*2/ *r*1 decreases from 2.74 to 2.12 at 298 K (Table 2). As a result, the degree of the charge split is reduced from $D^{0.75+}D^{0.25+}$ to $D^{0.65+}D^{0.35+}$. In the charge-ordered state, both kinds of dimerization ratio of the AsF_6 complex (*r*2/*r*1 = 1.94, *r*4/*r*3 = 1.34) are smaller than those of the PF_6 complex (2.01, 1.39). With a lowered temperature, the reduction rate of the dimerization ratio {[(*r*2/*r*1) (30 K)]/[(*r*2/*r*1) (298 K)] = 0.92 and [(*r*4/*r*3) (30 K)]/[(*r*2/*r*1) (298 K)]} = 0.63 for the AsF_6 salt is also smaller than those (0.73 and 0.51) for the PF_6 salt.

Figure 2. Checkerboard-type charge ordering by crystal structure analysis for *β*-(*meso*-DMBEDT-TTF)$_2$AsF$_6$. The charge-rich and charge-poor molecules are indicated by red and blue. (**a**) *r*1, *r*2, *r*3, *r*4, *p*1, *p*2, *q*1, *q*2, *q*3, and *q*4 are transfer integrals. (**b**) The double, single, and dotted lines indicate the strength of intermolecular interactions.

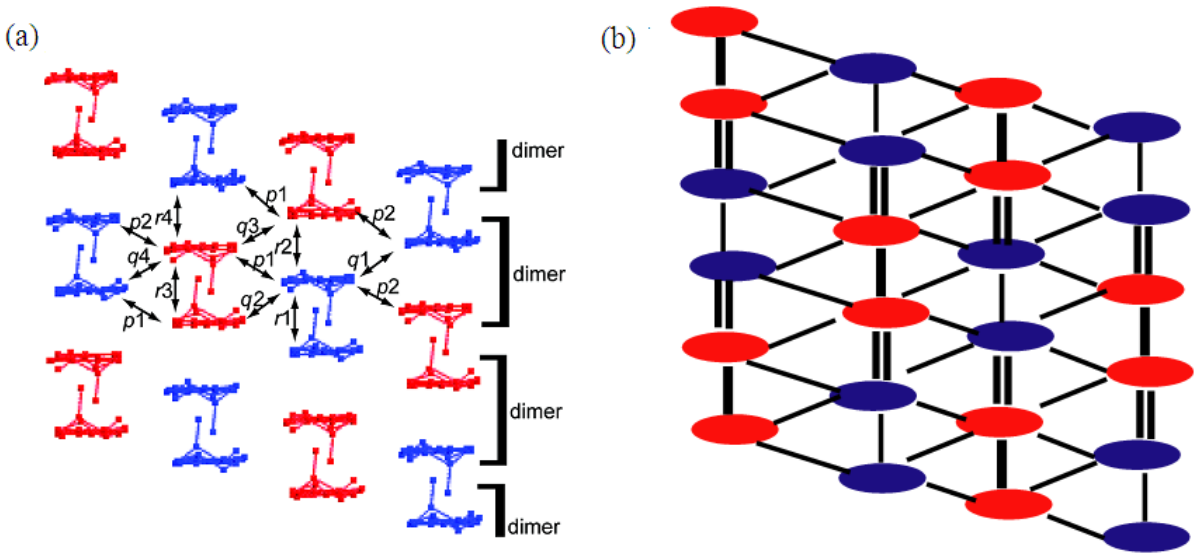

Table 1. Charge estimation of the TTF moiety of the charge-rich and poor donors by bond length analysis at 30 K for *β*-(*meso*-DMBEDT-TTF)$_2$AsF$_6$. The tentative charge *δ*1 was calculated by an equation from the literature: {*δ*1 = 6.347*[(b1 + b2 + b3 + b4)/4 + (c1 + c2 + c3 + c4)/4 − a− (d1 + d2)/2)] − 7.463} [10]. The real charge *δ*2 was estimated to be +0.65 and +0.35 by normalization of the *δ* 1 values, respectively. The sum of the two *δ*2 values was set to be +1.

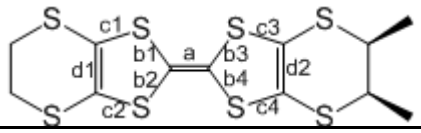

	a (Å)	**b1** (Å) **b2** (Å) **b3** (Å) **b4** (Å)	**c1** (Å) **c2** (Å) **c3** (Å) **c4** (Å)	**d1** (Å) **d2** (Å)	***δ*1**	***δ*2**
charge-rich donor	1.379(4)	1.735(3) 1.728(3) 1.722(3) 1.741(2)	1.748(3) 1.743(3) 1.752(3) 1.751(3)	1.354(4) 1.350(4)	+0.76(3)	+0.65(3) [=0.76(3)/ (0.76(3)+0.41(3))]
charge-poor donor	1.354(4)	1.745(2) 1.751(3) 1.753(4) 1.740(2)	1.749(4) 1.757(3) 1.760(3) 1.757(4)	1.357(4) 1.350(4)	+0.41(3)	+0.35(3) [=0.41(3)/ (0.76(3)+0.41(3))]

Table 2. Transfer integrals (× 10^{-2} eV) of *β*-(*meso*-DMBEDT-TTF)$_2$X (X = PF_6 [4,6], AsF_6).

Direction	298 K		Direction	11.5 K	30 K
	PF_6	**AsF_6**		**PF_6**	**AsF_6**
*r*1	8.24	9.86	*r*1	12.6	12.9
r 2	22.6	20.9	*r*2	25.3	25.1
r 3	-	-	*r*3	18.2	18.7
r 4	-	-	*r*4	25.3	25.1
*p*1	−4.75	−4.89	*p*1	−4.4	−4.3
*p*2	-	-	*p*2	−6.1	−6.1
*q*1	4.38	4.03	*q*1	3.7	3.7
*q*2	11.5	10.7	*q*2	10.7	10.6
*q*3	-	-	*q*3	4.2	4.3
*q*4	-	-	*q*4	10.7	10.6
*r*2/*r*1	2.74	2.12	*r*2/*r*1	2.01	1.94
*r*4/*r*3	-	-	*r*4/*r*3	1.39	1.34
Ref.	[4]	this work	-	[6]	this work

Table 3. Band parameters of *β*-(*meso*-DMBEDT-TTF)$_2$X (X = PF_6, AsF_6) and *κ*-(BEDT-TTF)$_2$X [X = $Cu(NCS)_2$, $Cu_2(CN)_3$] at 298 K. The parameters W_u, W_L, W, E_g, ΔE, and $W_u/\Delta E$ denote the upper band, lower band, total bandwidth, energy gap between upper and lower bands, ΔE = 2*(intradimer transfer integral), and $W_u/\Delta E$.

	W_U	W_L	W	Eg	ΔE	$W_U/\Delta E$	ref.
β-(*meso*-DMBEDT-TTF)$_2PF_6$	0.50	0.40	0.93	0.02	0.45	1.11	[4]
β-(*meso*-DMBEDT-TTF)$_2AsF_6$	0.51	0.43	0.92	0	0.42	1.23	this work
κ-(BEDT-TTF)$_2Cu(NCS)_2$	0.57	0.36	1.08	0.16	0.46	1.24	[11–13]
κ-(BEDT-TTF)$_2Cu_2(CN)_3$	0.50	0.33	1.00	0.17	0.45	1.11	[13]

In order to elucidate the electronic state at 298 K, the correlation parameters $W_U/\Delta E$ [W_U: upper band width, ΔE: on-site Coulomb repulsion energy = 2 * (intradimer transfer energy)] of the obtained *β*-(*meso*-DMBEDT-TTF)$_2$X (X = PF_6, AsF_6) at 298 K are shown in Table 3. The parameters $W_U/\Delta E$ are calculated to be 1.11–1.23, which is comparable to those of *κ*-(BEDT-TTF)$_2$X {1.24 for X = $Cu(NCS)_2$ [11–13], 1.11 for $Cu_2(CN)_3$ [13]}. Therefore, the complexes *β*-(*meso*-DMBEDT-TTF)$_2$X (X = PF_6, AsF_6) might be in the dimer state at 298 K.

Moreover, the enhancement of the mid-infrared conductivity hump in the optical spectra for *β*-(*meso*-DMBEDT-TTF)$_2PF_6$, which originates from a transition between lower and upper Mott Hubbard bands, demonstrates experimentally that the complex is in the dimer state from room temperature to 75 K [14]. Since the lower bandwidth of *β*-(*meso*-DMBEDT-TTF)$_2$X is wider than that of *κ*-(BEDT-TTF)$_2$X, the gap between the upper and lower bands (Eg) is 0–0.02 eV and the complex *β*-(*meso*-DMBEDT-TTF)$_2PF_6$ shows weak metallic behavior from room temperature to 75 K at an ambient pressure (Figure 1, [4,7]). Below 75 K, the dimer optical peak stops growing and the charge-ordering band starts to increase [14].

2.2. Pressure-Induced Superconductivity of β-(meso-DMBEDT-TTF)$_2$AsF$_6$

Figure 3 shows the temperature dependences of resistivities under an ambient and a pressurized condition for *β*-(*meso*-DMBEDT-TTF)$_2$AsF$_6$. This complex with 0.1 ohm cm at 300 K exhibits weak metallic behavior down to 90 K and is transformed into the insulating state. Compared with *β*-(*meso*-DMBEDT-TTF)$_2$PF$_6$ [4,7], the resistivity at room temperature is similar, 0.1 ohm cm, but the metal- insulator transition is broader. The rapid increase of the resistivity was suppressed under 0.19 GPa and a distinct resistivity drop at 4.2 K was observed under 0.38 GPa. As pressure is applied, the temperature of the resistivity drop decreases monotonically with −4.7 K/GPa, which is similar to that of *β*-(*meso*-DMBEDT-TTF)$_2$PF$_6$, −4.5 K/GPa [7]. As shown in Figure 4, the resistivity drop under 0.38 GPa was suppressed by applying a magnetic field and proved to be the superconducting (SC) transition. This magnetoresistance reached +32% just above the transition temperature of 4.6 K under 9 T, which might have been due to the Pauli Blockade originating from CO [15], similar to the case of *β*-(*meso*-DMBEDT-TTF)$_2$PF$_6$ [7].

Figure 3. (**a**) Temperature dependence of electrical resistivity (**a**) from ambient pressure to 1.5 GPa and (**b**) under 0.38–0.6 GPa for *β*-(*meso*-DMBEDT-TTF)$_2$AsF$_6$.

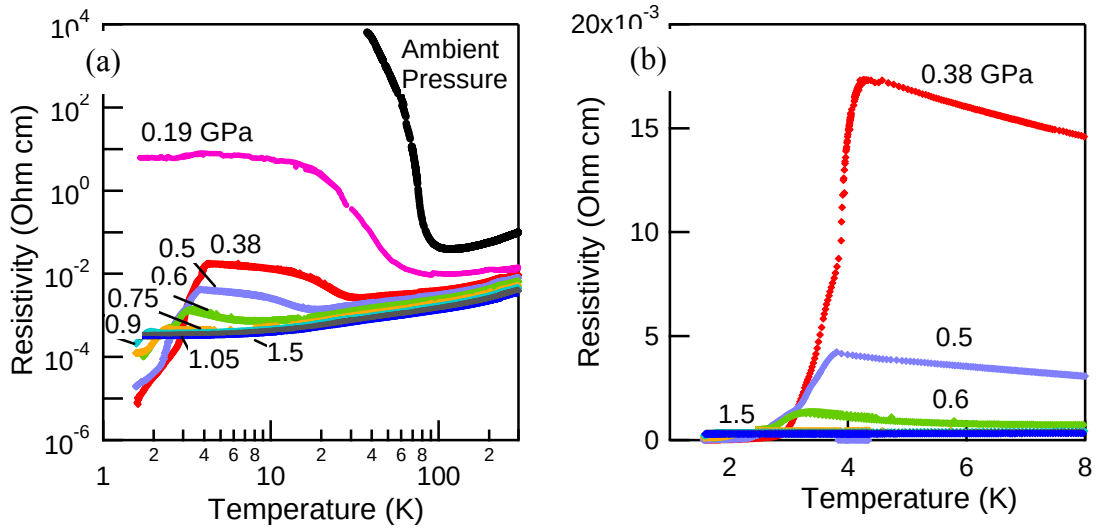

Figure 5(a) shows the temperature dependence of resistivity under pressure below 30 K. The analysis of $\rho \propto T^{\alpha}$ was carried out under several pressures in the temperature range of $2 < T < 20$ K. The exponent α is 2 when the electronic state is in the Fermi liquid nature. Near the superconducting state, α is calculated to be 1.3 under 0.9 GPa. The power α increases almost linearly with application of pressure. The pressure dependence is $d\alpha/dP$ = 0.6 K/GPa, which is much faster than those of (TMTTF)$_2$X (X = PF$_6$, AsF$_6$) with 0.15–0.19 K/GPa [16]. The system at 1.5 GPa is non-Fermi liquid (NFL) with α = 1.7 and might be realized to be the Fermi liquid above 2.5 GPa if the linear extrapolation of the pressure dependence is assumed.

The phase diagram of *β*-(*meso*-DMBEDT-TTF)$_2$AsF$_6$ is elucidated in Figure 5(b). At an ambient pressure, the insulating state below the transition temperature is the checkerboard-type charge-ordered state. Upon the application of pressure, the metal-insulator transition temperatures are lowered and the

distinct superconducting transition appears under 0.38–0.9 GPa at 4.2–1.9 K. For both complexes *β*-(*meso*-DMBEDT-TTF)$_2$X (X = PF_6 [7] and AsF_6), the SC states compete with the charge-ordered states over certain pressure ranges.

Figure 4. Temperature dependence of electrical resistivity under a magnetic field for *β*-(*meso*-DMBEDT-TTF)$_2$$AsF_6$.

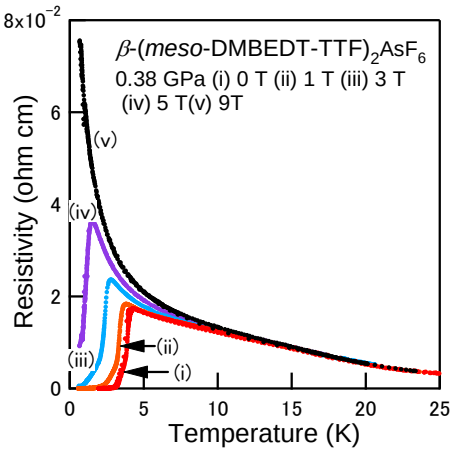

Figure 5. (**a**) Temperature dependence of electrical resistivity under pressure and (**b**) pressure dependence of T_c, T_{min}, and a [the superconducting transition temperature, the temperature of resistivity minimum, and $\rho \propto T^{\alpha}$ in Figure 5(a)] for *β*-(*meso*-DMBEDT-TTF)$_2$$AsF_6$. In (**b**) CO and SC denote the charge-ordered state and the superconducting state.

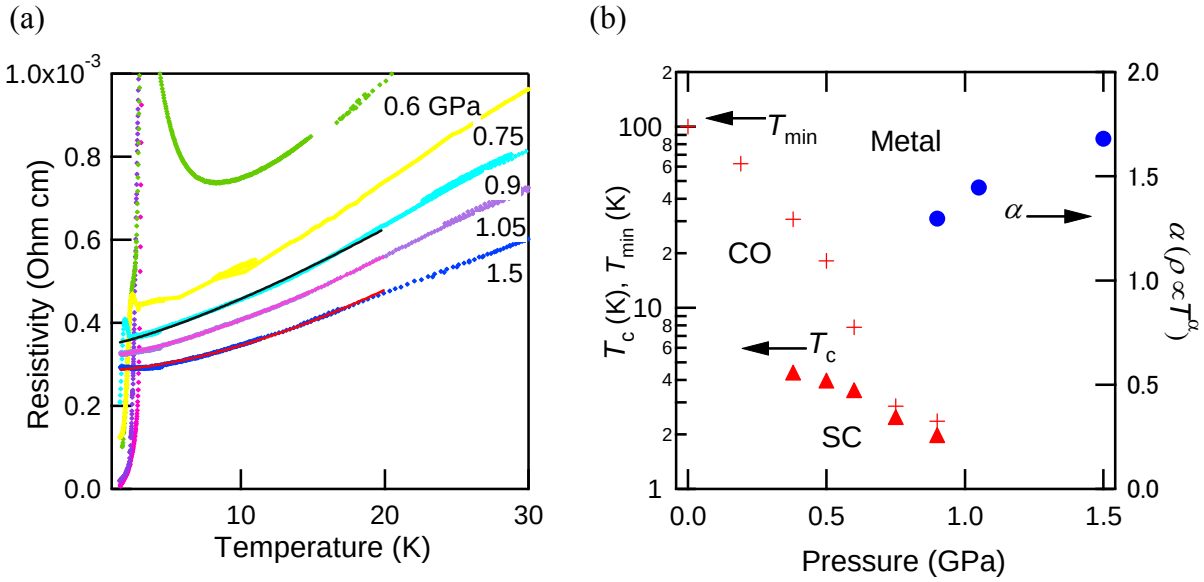

2.3. Magnetic Susceptibility of β*-(meso-DMBEDT-TTF)$_2$X (X = PF_6 and AsF_6)*

Under ambient pressure, the dimer state of the titled complexes is developed with lowering temperature and is suddenly transformed into the checkerboard-type charge-ordered state with accompanying metal-insulator transition around 75–90 K. In order to clarify the electronic state of *β*-(*meso*-DMBEDT-TTF)$_2$X (X = PF_6 and AsF_6), the measurements of static magnetic susceptibilities

were carried out as shown in Figure 6. The static magnetic susceptibilities at 300 K for *β*-(*meso*-DMBEDT-TTF)$_2$X (X = PF_6 and AsF_6) are 5.5 × 10^{-4} and 5.3 × 10^{-4} emu mol^{-1}, respectively. These values are similar to those of the electron-correlated molecular conductors, such as the dimer-Mott molecular conductors *κ*-(BEDT-TTF)$_2$X {X = Cu(NCS)$_2$, Cu[N(CN)$_2$]Br, Cu[N(CN)$_2$]Cl}, 4.2–4.5 × 10^{-4} emu mol^{-1} [17], and the charge-ordered conductor, *θ*-(BEDT-TTF)$_2$RbZn(SCN)$_4$, 6.0 × 10^{-4} emu mol^{-1} [18]. With lowering temperatures, the susceptibilities decrease gradually and drop from 4.7–4.5 × 10^{-4} emu mol^{-1} around 80 K to 3.1–2.7 × 10^{-4} emu mol^{-1} around 60 K. The susceptibility of the PF_6 complex below 80 K was well fitted by the following, as shown by the solid line in Figure 6:

Figure 6. Temperature dependences of magnetic susceptibilities for *β*-(*meso*-DMBEDT-TTF)$_2$X (X = PF_6 and AsF_6). The solid line is the fitting curve (see text).

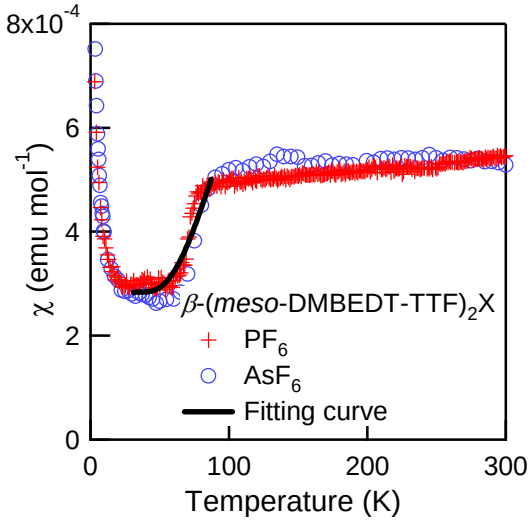

$$\chi = 0.95 * ST_1 + 0.044 * L_2 + 0.006 * Curie_1$$

$$ST_1 = 2Ng^2\mu_B{}^2/kT(3 + exp(-2J_1/kT))$$

$$L_2 = Ng^2\mu_B{}^2 S(S+1)/kT * (3 + 3/(T/J_2) + 1.5001/(T/J_2)^2 + 0.4999/(T/J_2)^3 + 0.0471/(T/J_2)^4 - 0.0453/(T/J_2)^5 + 0.00017797/(T/J_2)^6)^{(-1)}$$

$$Curie_1 = Ng^2\mu_B{}^2 S(S+1)/3kT$$

$$N;\ Avogadro's\ Number,\ \mu_B;\ BohrMagneton,\ S = 1/2, J_1 = 170K, J_2 = 45K$$

The contributions of ST_1, L_2, and $Curie_1$ denote the susceptibilities based on a singlet-triplet model [19], a two-dimensional Heisenberg model [20], and Curie law. The drop of the susceptibility below 80 K is mainly fitted by the singlet-triplet model. Recently, Okazaki and Terasaki *et al.* reported that the infrared imaging measurements of several samples indicated the inhomogeneity of the charge-ordered and the dimer states even below 80 K [14]. The contribution of the dimer state by the two-dimensional Heisenberg model showed good agreement with the experimental data. At low temperatures, the 0.6% Curie contribution (S = 1/2 and g = 2) is due to the impurity. The behaviors of the PF_6 and AsF_6 complexes are similar. The measurements of magnetic susceptibilities indicate that

the ground state would be the spin-gapped state, which is consistent with the behavior by the NMR measurement [21].

In Section 2.1, the checkerboard-type charge ordering in the PF_6 and AsF_6 complexes is described. The charge disproportionation is usually caused by the electron-electron repulsion in the closest donor pair [2]. In this case, the dimer ($D^{0.5+}$ $D^{0.5+}$) at 298 K is transformed into the charge-disproportionated pair ($D^{0.65+}D^{0.35+}$) to construct ··$D^{0.65+}$)($D^{0.65+}D^{0.35+}$)($D^{0.35+}$·· in the stacking direction below 70 K. This charge distribution induces not only the checkerboard-type charge ordering with accompanying lattice modulation, but also the spin-singlet state at the same transition temperature. This spin-gapped state, namely the two-dimensional Spin Peierls state, is the origin of the checkerboard-type charge ordering and the characteristic feature of the strong electron-phonon coupling for molecular materials.

The electronic state of the titled complexes can be discussed by the spin-singlet paired-electron crystal (PEC) model in the two-dimensional strongly correlated quarter-filled band on the anisotropic triangular lattice [22] [Figure 2]. In the moderate or strong spin and charge frustrated region, the checkerboard-type charge-ordering, wherein the pairs of the charge-rich sites are separated by the pairs of the charge-poor sites, affords the spin-singlet state. The phase diagram as a function of onsite and intersite Coulomb interactions as well as the electron-phonon coupling is also discussed in this model. Moreover, it is speculated that the spin-bonded pairs of the PEC can become mobile for stronger frustration, giving rise to a paired-electron liquid. The titled complexes seem to be explained by the PEC model. The appearance of the checkerboard-type charge ordering in the two-dimensional quarter-filled band on the anisotropic triangular lattice at 70 K affords the spin-gapped state by the static magnetic susceptibility and the NMR measurements at low temperatures. The transfer integrals of charge-rich sites [$r3$ = 18.2 (the PF_6 complex) and 18.7 × 10^{-2} eV (the AsF_6 complex)] are larger than those of charge-poor sites ($r1$ = 12.6 and 12.9 × 10^{-2} eV) in the charge-ordered and spin-gapped state for *β*-(*meso*-DMBEDT-TTF)$_2$X (X = PF_6 and AsF_6), respectively (Table 2). Under the pressurized condition, both complexes exhibit superconductivity, which was attributed to a paired-electron liquid. The PEC model can be applied for not only *β*-(*meso*-DMBEDT-TTF)$_2$X (X = PF_6 and AsF_6), but also thiospinel $CuIr_2S_4$ [23] with the charge-ordered and the spin-dimerized transition at 230 K, and triclinic $EtMe_3P[Pd(dmit)_2]_2$ [24] with the charge-ordered and the spin-gap transition.

3. Experimental Section

Single crystals of *β*-(*meso*-DMBEDT-TTF)$_2$X (X = PF_6 and AsF_6) were prepared by the electrocrystallization method of the 0.5 μA constant current with *meso*-BEDT-TTF (5 mg; anode side) and TBA·X (X = PF_6 and AsF_6, 15 mg × 2; both anode and cathode sides) in chlorobenzene (10 mL) over a week. The obtained black plate crystals were washed with ethanol and dried.

Reflection data were collected with a Rigaku Mercury CCD (Mo-K_α, λ = 0.71069 Å) at room temperature at the Institute for Solid State Physics and at 30 K at the Institute for Molecular Science. The crystal structures were solved by direct methods and refined with the full-matrix least-squares technique using Crystal Structure software (ver. 4.0.1; Rigaku Co. and Rigaku Americas Co.). Anisotropic thermal parameters were applied to all non-hydrogen atoms. The hydrogen atoms were generated geometrically (C-H = 0.960 Å). The crystal data of *β*-(*meso*-DMBEDT-TTF)$_2$$AsF_6$ at 298 K were as follows: $C_{24}H_{24}S_{16}AsF_6$ Fw 1014.33, triclinic, *P1*-(No. 2), *a* = 9.162 (4) Å, *b* = 15.738(8) Å,

c = 6.742(3) Å, α = 91.14(1)°, β = 109.811 (9)°, γ = 89.05(1)°, V = 914.3(7) Å^3, Z = 1, D_{calc} = 1.842 g/cm^3, $R_1(I > 2\sigma)$ = 0.0462, wR_2 (all data) = 0.0968, and goodness of fit = 0.680; the data at 30 K were as follows: triclinic, *P1*-(No. 2), a = 9.035(14) Å, b = 13.073(2) Å, c = 16.704(3) Å, α = 106.185(3)°, β = 98.019 (2)°, γ = 108.917(3)°, V = 1734.1(5) Å^3, Z = 2, D_{calc} = 1.943 g/cm^3, $R_1(I > 2\sigma)$ = 0.0372, wR_2 (all data) = 0.0558, and goodness of fit = 1.005.

The molecular orbitals were calculated by the extended Hückel method based on the crystal structure data. The transfer integrals were obtained based on the calculated molecular orbitals. The band calculation was carried out by tight-binding approximation utilizing the obtained transfer integrals [25].

The electrical resistivities under ambient and pressurized conditions utilizing PPMS (Physical Properties Measurement System; Quantum Design) were measured by the four-probe method with a carbon paste as contacts in the range of 2–300 K and 0–9 T. The 10 μA current was passed along the crystal long *c*–axis (1.0 × 0.2 × 0.02 mm^3) and the external magnetic field was applied to the *c* axis. The pressure was applied with a BeCu-NiCrAl clamp cell with Daphne 7373 as a pressure medium. The resistivies of the sample and the Pb wire were measured simultaneously. The superconducting transition temperature of Pb wire indicates the applied pressure [26].

The magnetic susceptibility was measured by an MPMS (Magnetic Property Measurement System; Quantum Design). The diamagnetic contributions of β-(*meso*-DMBEDT-TTF)$_2$X (X = PF_6 and AsF_6) were estimated by adding the diamagnetic contributions for anions by Pascal's law [27] and the measured value [28] of BEDT-TTF to be 5.06 × 10^{-4} and 5.11 × 10^{-4} emu mol^{-1}, respectively.

4. Conclusions

The metallic state in the two-dimensional strongly correlated system on the anisotropic triangular lattice of β-(*meso*-DMBEDT-TTF)$_2$X (X = PF_6 and AsF_6) is transformed to the insulating checkerboard-type charge-ordered and spin-gapped state demonstrated by the crystal structure analysis at low temperatures and with magnetic susceptibility measurement. Upon application of pressure, the SC state appears, which competes with the charge-ordered state within a certain pressure range. The finding that the spin-bonded electron pairs stay in the checkerboard-type charge-ordered state at an ambient pressure and becomes mobile in the frustrated state on the triangular lattice under pressure is discussed based on the paired-electron crystal (PEC) model.

Acknowledgments

We thank T. Clay for his helpful discussion. This work was supported by Grants-in Aid for Scientific Research (B) (No. 20340087) and on Innovative Areas of Molecular Degrees of Freedom (No. 20110007) from the Ministry of Education, Culture, Sports, Science and Technology. We thank the Instrument Center for the Institute for Molecular Science for allowing us to use the X-ray diffractometer with Rigaku Mercury CCD at 30 K.

References

1. Fukuyama, H. Physics of Molecular Conductors. *J. Phys. Soc. Jpn.* **2006**, *75*, doi: 10.1143/JPSJ.75.051001.
2. Seo, H.; Hotta, C.; Fukuyama, H. Toward Systematic Understanding of Diversity of Electronic Properties in Low-dimensional Molecular Solids. *Chem. Rev.* **2004**, *104*, 5005–5056.
3. Kimura, S.; Suzuki, H.; Maejima, T.; Suto, M.; Yamashita, K.; Ichikawa, S.; Mori, H.; Moriyama, H.; Mochida, T.; Nishio, Y.; Kajita, K. Crystal Structures and Electrical Conductivities Controlled by CH/n interactions. *J. Phys. IV Fr.* **2004**, *114*, 521–522.
4. Kimura, S.; Maejima, T.; Suzuki, H.; Chiba, R.; Mori, H.; Kawamoto, T.; Mori, T.; Moriyama, H.; Nishio, Y.; Kajita, K. A New Organic Superconductor *β*-(*meso*-DMBEDT-TTF)$_2$PF$_6$. *Chem. Commun.* **2004**, 2454–2455.
5. Kimura, S.; Suzuki, H.; Maejima, T.; Mori, H.; Yamaura, J.; Kakiuchi, T.; Sawa, H.; Moriyama, H. Checkerboard-Type Charge-Ordered State of a Pressure-Induced Superconductor, *β*-(*meso*-DMBEDT-TTF)$_2$PF$_6$. *J. Am. Chem. Soc.* **2006**, *128*, 1456–1457.
6. Mori, H. Materials Viewpoint of Organic Superconductors. *J. Phys. Soc. Jpn.* **2006**, *75*, doi: 10.1143/JPSJ.75.051003.
7. Morinaka, N.; Takahashi, K.; Chiba, R.; Yoshikane, F.; Niizeki, S.; Tanaka, M.; Yakushi, K.; Koeda, M.; Hedo, M.; Fujiwara, T.; *et al.* Superconductivity Competitive with Checkerboard-type Charge Ordering in Organic Conductor *beta*-(*meso*-DMBEDT-TTF)$_2$PF$_6$. *Phys. Rev. B* **2009**, *80*, doi: 10.1103/PhysRevB.80.092508.
8. Niizeki, S.; Yoshikane, F.; Kohno, K.; Takahashi, K.; Mori, H.; Bando, Y.; Kawamoto, T.; Mori, T. Dielectric Response and Electric-Field-Induced Metastable State in an Organic Conductor *β*-(*meso*-DMBEDT-TTF)$_2$PF$_6$. *J. Phys. Soc. Jpn.* **2008**, *77*, doi: 10.1143/JPSJ.77.073710.
9. Tanaka, M.; Yamamoto, K.; Uruichi, M.; Yamamoto, T.; Yakushi, K.; Kimura, S.; Mori, H. Infrared and Raman Study of the Charge-Ordered State in the Vicinity of the Superconducting State in the Organic Conductor *β*-(*meso*-DMBEDT-TTF)$_2$PF$_6$. *J. Phys. Soc. Jpn.* **2008**, *77*, doi: 10.1143/JPSJ.77.024714.
10. Guionneau, P.; Kepert, C.J.; Bravic, G.; Chasseau, D.; Truter, M.R.; Kurmoo, M.; Day, P. Determining the Charge Distribution in BEDT-TTF Salts. *Synth. Metals* **1997**, *86*, 1973–1974.
11. Oshima, K.; Mori, T.; Inokuchi, H.; Urayama-Mori, H.; Yamochi, H.; Saito, G. Shubnikov-de Haas Effect and the Fermi Surface in an Ambient Pressure Organic Superconductor [bis(ethylenedithiolo)tetrathiafulvalene]$_2$Cu(NCS)$_2$. *Phys. Rev. B* **1988**, *38*, 938–941.
12. Mori, H. Overview of Organic Superconductors. *Int. J. Mod. Phys. B* **1994**, *8*, doi: 10.1142/S0217979294000026.
13. Komatsu, T.; Matsukawa, N.; Inoue, T.; Saito, G. Realization of Superconductivity at Ambient Pressure by Band-filling Control of *κ*-(BEDT-TTF)$_2$Cu$_2$(CN)$_3$. *J. Phys. Soc. Jpn.* **1996**, *65*, 1340–1365.
14. Okazaki, R.; Terasaki, I.; Mori, H. The University of Tokyo, Japan. Private communication, 2012.

15. Takahide, Y.; Konoike, T.; Enomoto, K.; Nishimura, M.; Terashima, T.; Uji, S.; Yamamoto, H.M. Large Positive Magnetoresistance of Insulating Organic Crystals in the Non-Ohmic Region. *Phys. Rev. Lett.* **2007**, *98*, doi: 10.1103/PhysRevLett.98.116602.

16. Itoi, M.; Araki, C.; Hedo, M.; Uwatoko, Y.; Nakamura, T. Anomalously Wide Superconducting Phase of One-Dimensional Organic Conductor $(TMTTF)_2SbF_6$. *J. Phys. Soc. Jpn.* **2008**, *77*, doi: 10.1143/JPSJ.77.023701.
17. Kanoda, K. Metal-Insulator Transition in κ-$(ET)_2X$ and $(DCNQI)_2M$: Two Contrasting Manifestation of Electron Correlation. *J. Phys. Soc. Jpn.* **2006**, *75*, doi: 10.1143/JPSJ.75.051007.
18. Mori, H.; Tanaka, S.; Mori, T. Systematic Study of the Electronic State in θ-type BEDT-TTF Organic Conductors by Changing the Electronic Correlation. *Phys. Rev. B* **1998**, *57*, 12023–12029.
19. Carlin, R.L. *Magnetochemistry*; Springer-Verlag: Berlin, Germany, 1986.
20. Lines, M.E. The Quadratic-Layer Antiferromagnet. *J. Phys. Chem. Solids* **1970**, *31*, 101–116.
21. Miyagawa, K.; Kanoda, K.; Mori, H. The University of Tokyo, Japan. Private communication, 2012.
22. Dayal, S.; Clay, R.T.; Li, H.; Mazumdar, S. Paired Electron Crystal: Order from Frustration in the Quarter-Filled Band. *Phys. Rev. B* **2011**, *83*, doi: 10.1103/PhysRevB.83.245106.
23. Radaelli, P.G.; Horibe, Y.; Gutmann, M.J.; Ishibashi, H.; Chen, C.H.; Ibberson, R.M.; Koyama, Y.; Hor, Y.-S.; Kiryukhin, V.; Cheong, S.-W. Formation of isomorphic Ir^{3+} and Ir^{4+} Octamers and Spin Dimerization in the spinel $CuIr_2S_4$. *Nature* **2002**, *416*, 155–158.
24. Yamamoto, T.; Nakazawa, Y.; Tamura, M.; Nakao, A.; Ikemoto, Y.; Moriwaki, T.; Fukaya, A.; Kato, R.; Yakushi, K. Intradimer Charge Disproportionation in *Triclinic*-$EtMe_3P[Pd(dmit)_2]_2$ (dmit: 1,3-Dithiole-2-thione-4,5-dithiolate). *J. Phys. Soc. Jpn.* **2011**, *80*, doi: 10.1143/JPSJ.80.123709.
25. Mori, T.; Kobayashi, A.; Sasaki, Y.; Kobayashi, H.; Saito, G.; Inokuchi, H. The Intermolecular Interaction of Tetrathiafulvalene and Bis(ethylenedithio)tetrathiafulvalene in Organic Metals. Calculation of Orbital Overlaps and Models of Energy-band Structures. *Bull. Chem. Soc. Jpn.* **1984**, *57*, 627–633.
26. Eiling, A.; Schilling, J.S. Pressure and Temperature Dependence of Electrical Resistivity of Pb and Sn from 1–300 K and 0–10 GPa-Use as Continuous Resistive Pressure Monitor Accurate Over Wide Temperature Range; Superconductivity Under Pressure in Pb, Sn and In. *J. Phys. F* **1981**, *11*, 623–639.
27. Iwasawa, Y., Eds. *Kagaku Binran Kisohen II*, *Version 5*; Maruzen: Tokyo, 2004, p. II-508.
28. Nozawa, K.; Sugano, T.; Urayama-Mori, H.; Yamochi, H.; Saito, G.; Kinoshita, M. Meissner Effect in an Organic Superconductor $(BEDT\text{-}TTF)_2[Cu(NCS)_2]$. *Chem. Lett.* **1988**, *17*, 617–620.